ANNUAL REVIEWS

Annual Review of Biophysics

Biomolecular Condensates in Contact with Membranes

Agustín Mangiarotti and Rumiana Dimova

Max Planck Institute of Colloids and Interfaces, Potsdam, Germany;
email: Rumiana.Dimova@mpikg.mpg.de

Annu. Rev. Biophys. 2024. 53:319–41

First published as a Review in Advance on February 15, 2024

The *Annual Review of Biophysics* is online at biophys.annualreviews.org

https://doi.org/10.1146/annurev-biophys-030722-121518

Keywords

biomolecular condensates, membrane wetting, membrane remodeling, protein phase separation, membraneless organelles, coacervates

Abstract

Biomolecular condensates are highly versatile membraneless organelles involved in a plethora of cellular processes. Recent years have witnessed growing evidence of the interaction of these droplets with membrane-bound cellular structures. Condensates' adhesion to membranes can cause their mutual molding and regulation, and their interaction is of fundamental relevance to intracellular organization and communication, organelle remodeling, embryogenesis, and phagocytosis. In this article, we review advances in the understanding of membrane–condensate interactions, with a focus on in vitro models. These minimal systems allow the precise characterization and tuning of the material properties of both membranes and condensates and provide a workbench for visualizing the resulting morphologies and quantifying the interactions. These interactions can give rise to diverse biologically relevant phenomena, such as molecular-level restructuring of the membrane, nano- to microscale ruffling of the condensate–membrane interface, and coupling of the protein and lipid phases.

Contents

1. INTRODUCTION

The cell cytoplasm is organized into membrane-bound and membraneless organelles, also known as biomolecular condensates. The latter represent liquid-like droplets that arise from the phase separation of intracellular compounds like proteins and genetic material (12, 21, 87). Biomolecular condensates not only provide a flexible means of modulating the spatiotemporal concentration of macromolecules, but also allow for the interaction and remodeling of membranous compartments through capillary forces (17, 39, 56, 69, 74, 76, 104, 105). In turn, membrane-bound organelles can regulate condensate dynamics and assembly (50, 93, 102).

Biomolecular condensate: a membraneless compartment made of one or more biological macromolecules concentrated relative to their surroundings

Phase separation: the process whereby a system reorganizes into two or more spatially different regions with distinct and uniform physical properties and/or compositions

The reconstitution of biomolecular condensates in vitro and their study through simulations have augmented our understanding of the molecular grammar of condensates and the factors that govern their formation and properties (2, 25, 44, 46, 73, 103). Interestingly, membrane wetting by condensates was first reported in model systems (54) and later observed in cells when the first descriptions of membraneless organelles were made (20, 98). This highlights the relevance of in vitro models as powerful predictive tools of the underlying physics in biological processes, since they allow the careful control of parameters to modulate the membrane–condensate interaction. Only recently has the importance of membrane interactions and remodeling by condensates come to light in the field of biology, thanks to the growing body of evidence demonstrating the crucial role of membrane–condensate contacts in processes like the biogenesis and fission of protein-rich granules in the endoplasmic reticulum (50, 93), signal transduction in T cells (96, 102), assembly of endocytic vesicles (29), and the formation of tight junctions (18), among others. To provide a biophysical background of these processes, we present an overview of various phenomena that

emerge from the interaction of membranes and condensates, outline models that explain these phenomena, and speculate about future directions in the field.

Capillary forces: forces that arise between fluid and solid surfaces in narrow spaces and that result in the fluid being drawn upward against the gravity due to adhesive and cohesive forces

2. PIONEERING STUDIES USING AQUEOUS TWO-PHASE SYSTEMS

2.1. Membranes and Aqueous Two-Phase Systems of Polyethylene Glycol and Dextran

The first studies on the effect of condensates on membranes (initiated by the group of C. Keating) were performed by encapsulating polymer mixtures of polyethylene glycol (PEG) and dextran into giant vesicles (41, 54, 61, 62). The schematic in **Figure 1*a*** summarizes the morphological

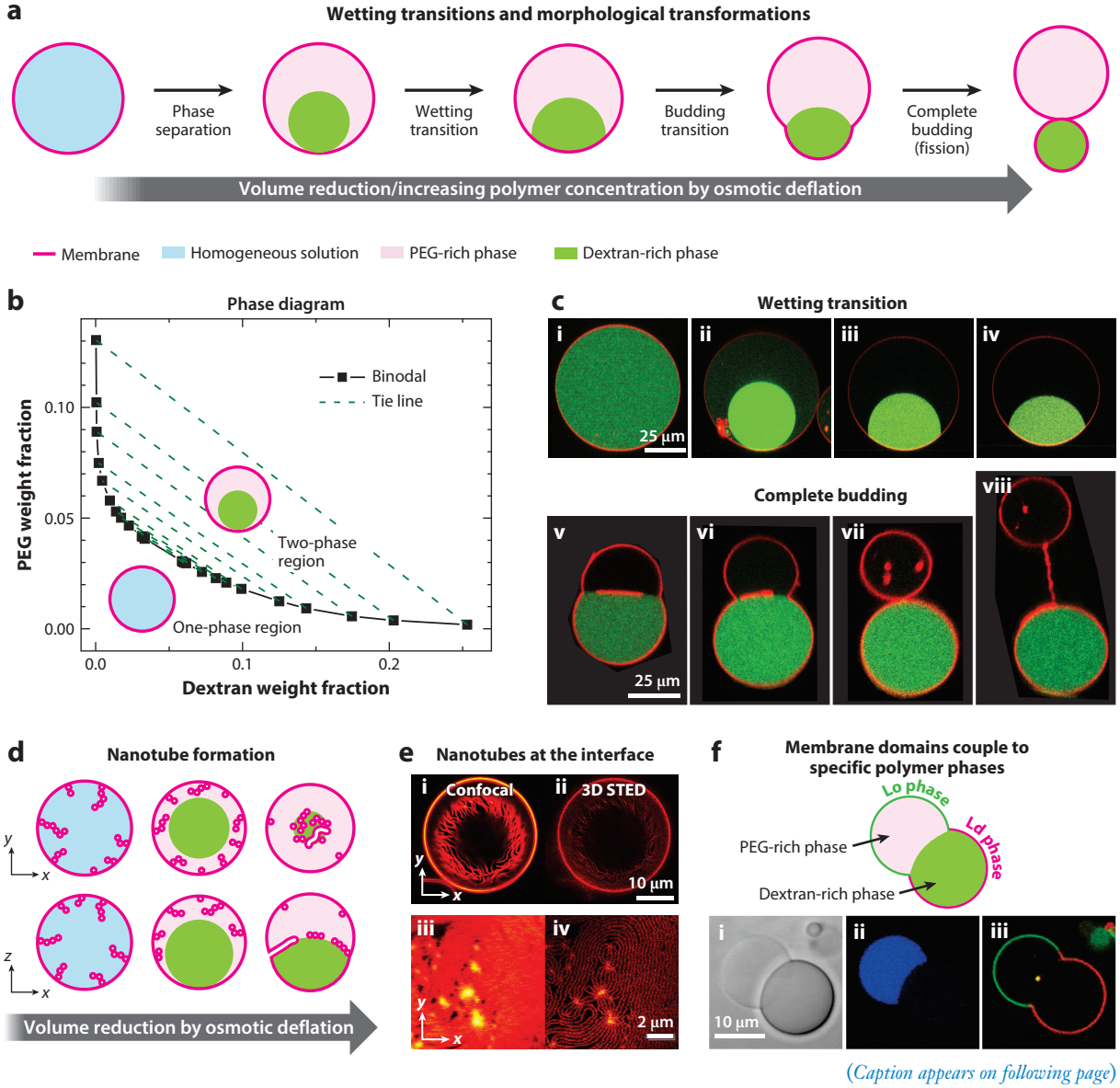

(*Caption appears on following page*)

Figure 1 (*Figure appears on preceding page*)

Liquid–liquid phase separation in aqueous two-phase systems (ATPSs) inside giant vesicles drives membrane morphological transformations. (*a*) Schematic summarizing the response of vesicles enclosing a polyethylene glycol (PEG)–dextran mixture under osmotic deflation. Panel adapted from Reference 33 with permission from the Royal Society of Chemistry. (*b*) Example phase diagram displaying the binodal and tie lines for a PEG–dextran ATPS (for details, see 60). Below the binodal, the polymer solution is homogeneous; it undergoes phase separation above the binodal. Panel adapted with permission from Reference 60; copyright 2012, American Chemical Society. (*c*) Fluorescence confocal images of giant vesicles containing PEG–dextran ATPSs. The membrane is shown in red, and a small fraction of dextran is labeled in green. (*i–iv*) As the external osmolarity is increased, the system undergoes a complete-to-partial wetting transition. Subpanels *i–iv* adapted with permission from Reference 54; copyright 2008, American Chemical Society. (*v–vii*) Increasing vesicle deflation causes the dextran-rich droplet to bud out, (*viii*) and can lead to fission of the enclosed droplets into two membrane-bound compartments with different content. Subpanels *v–viii* adapted with permission from Reference 53; copyright 2012, *The Journal of Physical Chemistry B*. (*d*) Schematic of three nanotube patterns observed when vesicle deflation produces a large excess area. The top row shows the horizontal views (xy cross sections), and the bottom row shows the vertical xz cross sections across the vesicle with increasing deflation. In all cases, the tubes are filled with external medium (*white*). The initial interior polymer solution is uniform (*blue*), and it phase separates upon deflation (*green and light pink*), undergoing complete to partial wetting of the membrane by the PEG-rich aqueous phase (*light pink*). With increasing deflation, the nanotubes explore the whole PEG-rich (*light pink*) droplet, avoiding wetting by the dextran-rich (*green*) one. Further deflating the vesicles, the membrane affinity to the dextran-rich phase increases (partial wetting), and the nanotubes adhere to the interface between the two aqueous droplets, gradually forming a crowded tube layer with further deflation. Panel adapted with permission from Reference 59; copyright 2016, American Chemical Society. (*e*) Confocal and 3D stimulated emission depletion (STED) images of the nanotubes adhered to the droplet interface. (*i–ii*) Only a fraction of the nanotubes is in focus due to the sphericity of the interface. (*iii–iv*) 3D STED allows one to resolve nanotubes at crowded interfaces. Panel adapted from Reference 108 (CC BY 4.0). (*f*) The presence of lipid-anchored polymers in phase-separated membranes can promote spatial coupling of membrane domains to specific polymer phases. In the confocal images bellow the schematic, the PEG-rich phase (*ii*, *blue*) is coupled to the liquid-ordered (Lo) domain (*iii*, *green*), and the liquid-disordered (Ld) domain (*red*) colocalizes with the dextran-rich phase. In the transmitted-light image (*i*), the dextran-rich phase appears darker because of the higher refractive index. Panel adapted with permission from Reference 23; copyright 2008, American Chemical Society.

transformations that can take place as a result of the interaction between these condensates and membranes. The liquid–liquid phase separation (LLPS) of these aqueous polymer solutions leads to what is known as an aqueous two-phase system (ATPS). The phase separation can be triggered by changes in the polymer concentration or temperature. An example phase diagram of a PEG–dextran ATPS is shown in **Figure 1*b***. At concentrations below the binodal, the solution is homogeneous; demixing takes place at concentrations above the binodal. The compositions of the resulting coexisting phases are defined by the crossings of the tie lines with the binodal. The tie lines can be obtained by measuring the densities of the coexisting phases (60). Knowing the phase diagram of these mixtures allows one to tune the polymer composition inside the vesicles and the resulting morphological transformations.

Liquid–liquid phase separation (LLPS): a type of phase separation in which a homogeneous solution reorganizes into two or more liquid phases with distinct composition

Aqueous two-phase systems (ATPSs): one example of LLPS; PEG–dextran solutions are the most popular ATPSs

Phase diagram: a graphical description of the phase behavior of a system as a function of one or more control parameters

2.2. Membrane Wetting and Remodeling

Liquid droplets at solid interfaces can adopt different shapes, forming zero or nonzero contact angles with respect to the surface; the affinity of the droplet to the surface is described by the Young's relation. A dewetted state is observed when the droplet remains spherical (like a drop on a lotus leaf) and not interacting with the surface; partial wetting is observed when the droplet forms a nonzero contact angle and partially spreads on the surface; and complete wetting takes place if the droplet spreads completely on the surface, forming a thin layer. There is an important difference between a droplet partially wetting a solid substrate and one partially wetting a membrane: In contrast to solid substrates, membranes are soft and have relatively low bending rigidity (32, 94) and can thus deform when in contact with the droplet (we provide a detailed description of the resulting geometries in Section 6). The interaction between the droplet and the membrane can be modulated by different factors, resulting in wetting transitions. Complete to partial wetting transition was first observed for giant unilamellar vesicles (GUVs) encapsulating PEG–dextran ATPSs (54), as shown in **Figure 1*a*,*c***. When the external osmolarity is raised, water is forced out

of the vesicles (osmotic deflation), increasing the concentration of the encapsulating polymers and triggering phase separation. The soft membrane deforms upon wetting, producing different biologically relevant processes such as budding, nanotube formation, compartmentalization, and fission, as shown in **Figure 1**. The PEG-rich phase is lighter than the dextran-rich one and has a lower refractive index, making the phases easily distinguishable by bright-field or phase-contrast microscopies. Fluorescently labeling the membrane and at least one of the polymers makes the system amenable to fluorescence microscopy characterization (see **Figure 1*c***). Deflation creates excess area, resulting in vesicle budding. Notably, the produced excess area can also be stored in membrane nanotubes (55, 59) (**Figure 1*d*,*e***). These nanotubes are stabilized by spontaneous curvature generated by weak adsorption of PEG on one side of the membrane (59) and can be retracted to the vesicle body under mild tensions applied with micropipettes (55). At first, the nanotubes protrude toward the vesicle interior and the PEG-rich phase. Then, to lower the interfacial tension, they accumulate at the interface between the two polymer-rich phases (55, 59) (**Figure 1*d*,*e***). Their diameters are below the optical resolution but are resolved with stimulated emission depletion (STED) super-resolution microscopy (108) (**Figure 1*e***). Tubes are nucleated from small buds, which grow into necklace-like tubes that, above a critical length, can transform into cylindrical ones (59). The membrane phase state modulates their diameter, with liquid-ordered (Lo) membranes presenting thicker tubes than liquid-disordered (Ld) ones (59), reflecting the higher bending rigidity of the former (40).

An interesting consequence of the membrane–condensate interaction is that membrane microdomains can localize to specific poles of Janus-like GUVs enclosing an ATPS (23). For ternary lipid mixtures displaying Lo–Ld phase separation, the (unspecific) affinity of one membrane phase to a specific polymer-rich phase can be tuned by including headgroup-modified (e.g., pegylated) lipids that partition to one of the membrane domains, pinning it to the respective (PEG-rich) phase, as shown in **Figure 1*f***. This approach exemplifies a primitive platform for cytoplasmic and membrane polarity in cells (23). Furthermore, when these systems are deflated, complete budding or fission can be achieved, providing a model for asymmetric cell division, with daughter vesicles having membrane and interior compositions that differ from one another (4).

3. MEMBRANE INTERACTIONS WITH SYNTHETIC COACERVATES

Complex coacervation is a type of LLPS that results from the attractive interaction of oppositely charged polyelectrolytes (90). In contrast to the ATPSs discussed in the previous section, which are examples of segregative phase separation (27), coacervation is an example of associative phase separation (90). The use of synthetic polypeptides that can form coacervates constitutes a convenient model system to mimic membraneless organelles. Given the simplicity of the handling of these molecules compared to the complex behavior of proteins and other biological macromolecules, polypeptides have been extensively used for the assembly of synthetic cells with different degrees of compartmentalization. Dekker and coworkers (30) showed that liposomes can provide a means of encapsulation and spatiotemporal control of the coacervate formation. Using passive proton permeation, reversible coacervation of encapsulated components can be produced in a controlled manner (47, 63) while tuning the interactions between the coacervates and the membrane (47), as shown in **Figure 2*a*,*b***. **Figure 2*a*** shows a schematic of a GUV encapsulating poly-L-lysine and ATP. Upshift of the external pH raises the pH inside the vesicle, and ATP becomes charged, triggering coacervation. Membrane–coacervate interactions can be tuned by electrostatic interactions, e.g., by including a negatively charged lipid that helps recruit the positively charged condensates to the membrane (47) (**Figure 2*b***, *left*). Another approach used to generate stronger droplet–membrane interactions is to physically anchor the coacervate into the membrane by using polymer-grafted lipids. In this case, hydrophobic interactions dominate, and coacervate nucleation

Binodal: in a phase diagram, the boundary line that outlines the region of two-phase coexistence

Tie line: line drawn in the phase coexistence region of a phase diagram for which the two ends at the binodal indicate the coexisting phase compositions

Young's relation: describes the relationship between the contact angle of a liquid droplet on a solid surface and the interfacial tensions among the liquid, solid, and surrounding gas

Bending rigidity: describes how flexible the membrane is; typical values are approximately 20 k_BT, where k_BT is the thermal energy (k_B is the Boltzmann constant, and T is the temperature)

Spontaneous curvature: represents a quantitative measure for the asymmetries between membrane leaflets and across the membrane; should be distinguished from molecular curvature, which is related to molecular geometry

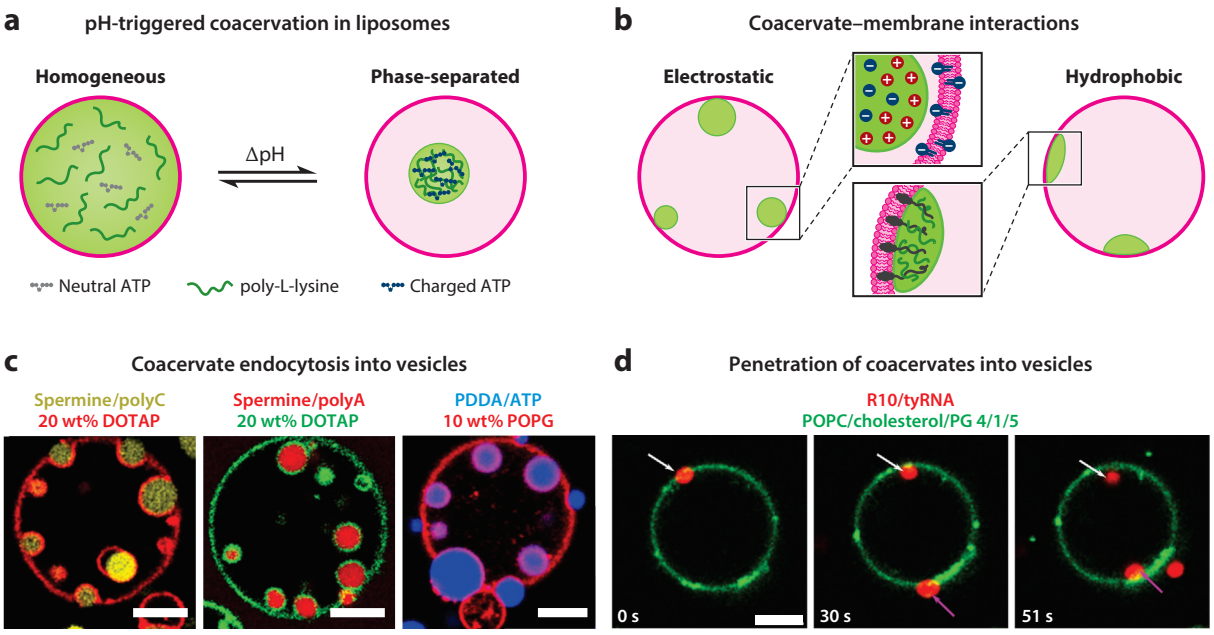

Figure 2

Coacervate–membrane interactions. (*a*) Coacervation can be triggered inside liposomes by passive proton permeation. The schematic shows an example of coacervation inside a vesicle containing poly-L-lysine and ATP: At low pH, the solution is homogeneous, and at basic pH, the ATP becomes charged, promoting coacervation. An example of this process can be found in Reference 47. (*b*) Surface charge can recruit coacervates to the membrane electrostatically (*left*). Incorporation of membrane-anchored molecules (*right*) that can form coacervates leads to wetting and remodeling of the membrane via hydrophobic interactions (see, e.g., 47). (*c*) Different coacervates can be engulfed by giant vesicles depending on the membrane and coacervate charges. Coacervate and membrane compositions are indicated. Scale bars are 5 μm. Panel adapted from Reference 65 (CC BY 4.0). (*d*) At certain conditions (specific coacervate and membrane surface charge difference and lipid partitioning in the coacervate), coacervates can penetrate the membrane and become internalized inside vesicles. Scale bars are 10 μm. Panel adapted from Reference 64 (CC BY 4.0).

Liquid-ordered (Lo) membranes: membranes that are fluid but exhibit denser lipid packing and reduced mobility than liquid-disordered membranes and that form specialized raft-like domains

Coacervates: liquid droplets formed by the interaction of two oppositely charged polyelectrolytes in solution

occurs at the membrane (47). As shown in **Figure 2*b*** (*right*), these coacervates wet and remodel the membrane. Following this first work on coacervate–membrane interactions, by using various complex coacervates and modifying the membrane surface charge, Spruijt, Huck, and coworkers (65) performed a systematic study of coacervate–membrane interactions. As shown in **Figure 2*c***, endocytosis of coacervates can occur for a variety of coacervates by tuning the membrane lipid charge composition. By modifying the interaction strength between coacervates and liposomes, Lu et al. (65) observed different morphologies for the coacervate–membrane system ranging from nonwetting to engulfment (endocytosis) and complete wetting. The same group found that, at a specific combination of zeta-potential difference between the coacervates and the liposomes and partition coefficient of lipids into the coacervates, coacervates can not only be engulfed but even penetrate the membrane and become internalized in the vesicles (64) (**Figure 2*d***). Using coarse-grained molecular dynamics simulations, Mondal & Cui (75) showed that, apart from membrane remodeling, coacervates can also facilitate local lipid demixing.

With a focus on the development of synthetic cells and using the approach of pH-driven coacervation, Love et al. (63) showed that enzymatic activity can be activated and modulated via coacervate formation inside GUVs. This study further exploited multicompartmentalization, providing a synthetic cell-like platform with pH-responsive and tunable enzymatic activity (63).

Coacervates can also serve as templates for membrane formation, allowing one to build a model system in which the complete interior consists of a coacervate model cytoplasm (6, 78, 79, 97, 106). These coacervate-supported membranes provide, in general, a high yield of coacervate droplets surrounded by apparently continuous membranes (79). Additionally, membranes provide a barrier against enzyme degradation of the coacervates (79) and can be used as artificial biomolecular microreactors for enzyme cascade reactions (106).

4. MEMBRANE REMODELING BY PROTEIN-RICH CONDENSATES

Similarly to the ATPSs and coacervates discussed in the previous sections, soluble proteins and nucleic acids can phase separate (in bulk), forming tridimensional droplets (condensates) that can adhere to, wet, and deform membranes (7, 69). In contrast, membrane-anchored proteins can exhibit phase separation resulting from lateral interactions at the membrane surface that leads to 2D clustering. This 2D phase separation occurs at concentrations lower than those required for bulk phase separation (14, 92, 93) because the membrane surface reduces the concentration threshold required for phase separation, promoting prewetting transitions in the undersaturation regime (84, 107). In this section, we summarize the different remodeling processes that can be generated by both bulk phase separation and 2D phase separation.

4.1. Membrane Remodeling by Nonanchored Protein Condensates

Figure 3*a–d* shows schematics of remodeling processes that can take place when membranes are wetted by condensates of nonanchored proteins. Upon contact with the membrane, the droplets can undergo two wetting transitions: from dewetting to partial wetting and from partial wetting to complete wetting (69) (**Figure 3*a*,*e***). These wetting transitions are easily modulated by changing the solution salinity or the membrane composition (69). The partial wetting regime is characterized by a range of affinities of the condensate to the membrane. At low affinity, the curved membrane segment in contact with the condensate points toward the vesicle interior, and when the affinity increases, it points toward the condensate; Section 6 provides a brief theoretical description based on the system geometry. In the high-affinity region of the partial wetting regime, if the membrane possesses excess area (more than the area required to establish the condensate interface and enclose the vesicle volume), then interfacial ruffling is observed (69) (**Figure 3*b*,*f***). If the excess area is reduced, e.g., via micropipette aspiration, then the ruffling is suppressed, and the interface is smoothed out (**Figure 3*c***).

The interfacial ruffling is a mutual remodeling process, in which complex finger-like protrusions are formed in both the condensate and the membrane. It is important to highlight that this phenomenon differs from tubulation triggered by spontaneous curvature generation, as in the case of ATPSs, where the tubes protrude toward the PEG-rich phase (see **Figure 1*d***), or in anchored protein condensation, as discussed in Section 4.3. In interfacial ruffling, the intricate ruffles arise from the gain in adhesion energy that overcompensates for the bending rigidity of the membrane (69). STED microscopy allows one to resolve the dimensions of the membrane protrusions that lie in the submicrometer range (**Figure 3*f***, *bottom*). As can be seen in **Figure 3*f***, the undulations do not have a characteristic length scale; their dimensions are defined by the membrane area available to form the protrusions and the volume constraints imposed by the sizes of the condensate and the vesicle (69).

Similarly to ATPSs and coacervates (65), protein condensate–membrane interactions can lead to complete droplet engulfment (69), as shown in **Figure 3*d*,*g***. Conditions of partial or complete wetting and sufficient membrane area to wrap the condensate are necessary prerequisites for engulfment. Dissipative particle dynamics simulations have demonstrated that condensates

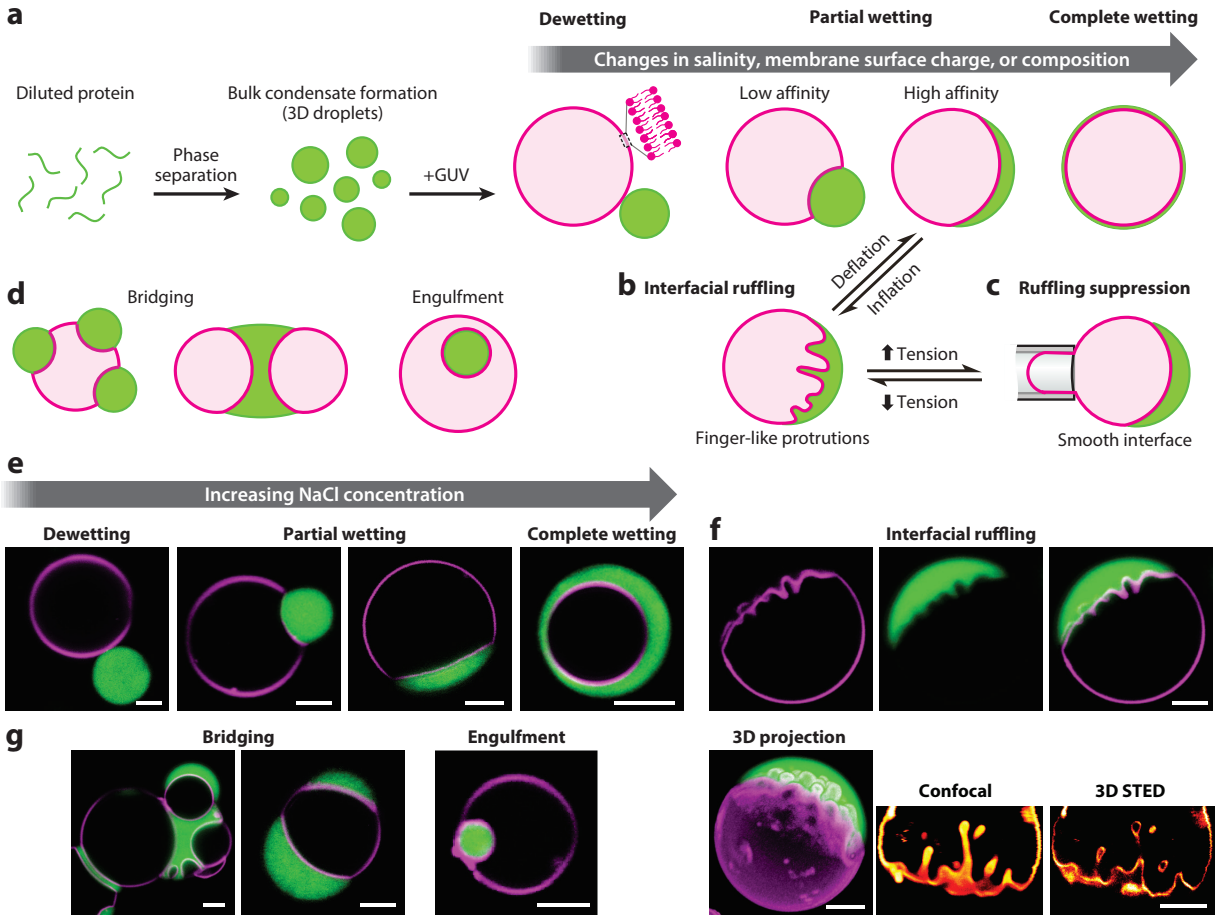

Figure 3

Membrane remodeling by nonanchored protein condensates. (*a–d*) Illustration of the observed wetting transitions and morphologies of the membrane–condensate system. Upon contact with the giant unilamellar vesicle (GUV) membrane (*magenta*), biomolecular condensates (*green*) can undergo two wetting transitions, from dewetting to partial wetting and from partial wetting to complete wetting. (*a*) Wetting transitions can be tuned by the ionic strength, membrane charge, and composition. (*b*) When excess membrane area is available, interface ruffling displaying finger-like protrusions can occur, (*c*) and ruffling can be suppressed when tension increases. (*d*) A vesicle can bridge several condensates, or a condensate can bridge two or more vesicles, while condensate engulfment can take place provided that there is enough membrane area. (*e,f*) Confocal and stimulated emission depletion (STED) images of GUVs (*magenta*) in contact with glycinin condensates (*green*). (*e*) Different wetting morphologies are observed when increasing the salinity. (*f*) Confocal cross sections (*top*) and 3D projection (*bottom left*) show that interfacial ruffling is a mutual remodeling process. 3D STED allows one to eliminate out-of-focus signals and resolve the membrane finger-like protrusions (*bottom right*). (*g*) Examples of a condensate bridging several vesicles or a vesicle bridging two condensates. On the right, an example of condensate engulfment is provided. Scale bars are 5 μm. Panels *a–c* and *e–g* adapted from Reference 69 (CC BY 4.0).

of polymers (with no particular intrinsic curvature) upon clustering can also sense curvature in bent membranes (5), suggesting that this could be a mechanism promoting endocytosis. Recently, Ghosh et al. (37) described different pathways for the endocytosis of nano-sized droplets in vesicles, identifying the transbilayer stress asymmetry and the line tension of the membrane–droplet contact line as the most relevant factors influencing the process. Endocytosis of several condensates can separate them from each other, preventing their coalescence. Furthermore, it can

regulate the diffusive exchange of molecules between the condensates and the bulk phase (106). In addition, a condensate can bridge two or more vesicles, or a vesicle can bridge several condensates (69) (**Figure 3*d*,*g***). Thus, wetting can lead to complex condensate–membrane architectures with different compartments (69).

4.2. Membrane Remodeling by Hollow Condensates

In 2017, Banerjee et al. (13) showed that changes in RNA or ribonucleoprotein concentrations could lead to phase separation within the condensates and the formation of hollow droplets. Later, with a combination of biophysical and computational tools, these hollow (or double-emulsion) condensates were found to exhibit local ordering, size-dependent permeability, and encapsulation capacity (3, 24). Moreover, they display similar properties to the isotropic droplets; e.g., they present mobility of the molecular species as assessed by fluorescence recovery after photobleaching, and can undergo coalescence (3). Presumably, the formation of hollow condensates is a general phenomenon for multicomponent systems of associative polymers displaying LLPS (3). It was shown to be a kinetic process in which the hollow structures emerge via dynamically arrested phase transitions (36).

The formation of hollow condensates from droplets rich in the soybean protein glycinin can be triggered by changes in the salt concentration inside the two-phase region of the phase diagram (24) (see **Figure 4*a***). This transition between isotropic droplets and hollow condensates can also be caused by pH or temperature changes (24). As shown in **Figure 4*b–d***, when these hollow condensates are in contact with membranes, they can also undergo wetting transitions and reshape the membrane just like isotropic droplets do (69). These structures offer additional means of compartmentalization that could be relevant in the organization of subcellular structures.

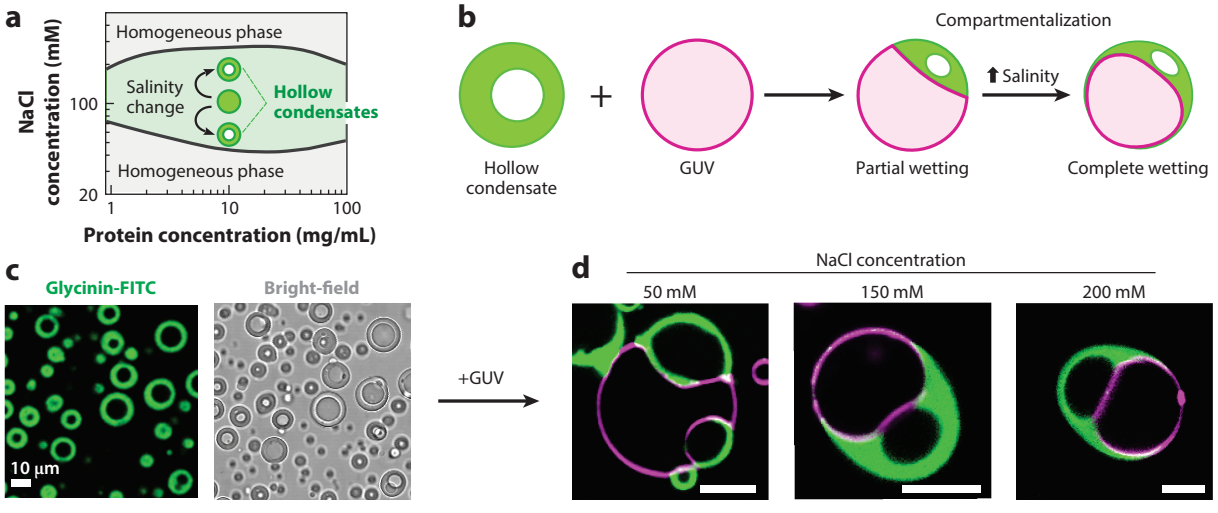

Figure 4

Hollow condensates can undergo wetting transitions and offer additional means for compartmentalization. (*a*) Schematic of the phase diagram of glycinin phase separation showing the pathways used to generate hollow condensates. From droplets, shifting the salinity to higher or lower NaCl concentration triggers phase separation within the droplets, forming hollow condensates. (*b*) Schematic summarizing the interaction of hollow condensates with vesicles. (*c*) Confocal and bright-field images of glycinin hollow condensates. (*d*) Hollow condensates (*green*) in contact with soy-phosphatidylcholine giant unilamellar vesicles (GUVs) (*magenta*) at the indicated NaCl concentrations undergo wetting transitions and allow for additional system compartmentalization. Scale bars are 10 µm. Panels *a*, *b*, and *d* adapted from Reference 69 (CC BY 4.0).

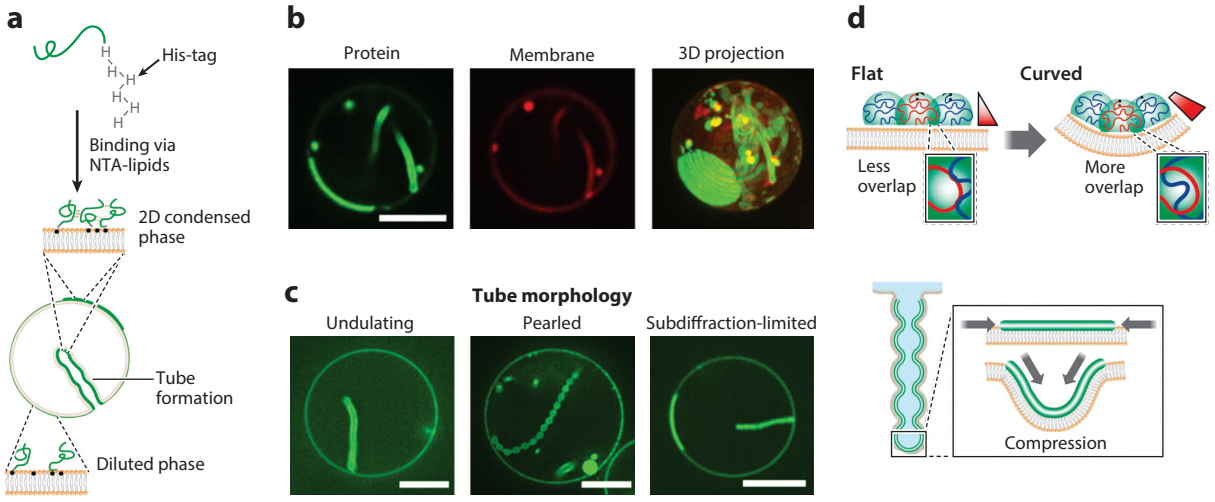

Figure 5

Membrane remodeling by lipid-anchored protein condensates. Lipid-anchored proteins and their lateral 2D phase separation promote membrane tubulation. (*a*) Schematic representing a histidine-tagged intrinsically disordered protein and its binding to membranes via NTA-lipids. Green segments on the vesicle membrane are phase separated proteins that promote inward tube formation. (*b*) Representative confocal images of giant unilamellar vesicles (GUVs) with anchored phase-separated FUS low-complexity domains (for further details, see 104). (*c*) Three kinds of membrane tube structures were observed: unduloids (see also panel *d*), pearl necklace–like, and subdiffraction-limited tubules. (*d*) Schematic illustrating the formation of tubules due to the compressive stresses emerging from protein liquid–liquid phase separation at the membrane surface. When the membrane is flat, unsatisfied protein–protein interactions become more numerous as distance from the surface increases and in this way create the driving force for membrane bending. If the membrane bends, then the overlap between the proteins is increased, enhancing interprotein interactions. Scale bars are 5 μm. Figure adapted from Reference 104; copyright 2021, National Academy of Sciences.

4.3. Membrane Remodeling by Lipid-Anchored Protein Condensates

When proteins are bound to the membrane, they can phase separate laterally even when the bulk solution does not display phase separation (14, 92, 93, 104). Proteins containing intrinsically disordered regions (IDRs) have large hydrodynamic radii that can generate steric pressure driving membrane bending (22). These proteins can establish weak multivalent interactions and undergo phase separation (21). Yuan et al. (104) showed that the FUS (Fused in Sarcoma) low-complexity domain can laterally phase separate at the membrane surface when it is bound to NTA (Ni-nitrilotriacetic-acid) lipids via the protein His-tag. The protein organizes into condensed (protein-rich) and diluted (protein-poor) phases on the 2D membrane surface, and the compressive stress generated by the condensed phase produces inward tubulation (104) (see **Figure 5*a***). This was also observed for other proteins (the low-complexity domain of hnRNPA2 and the RGG domain of LAF-1), suggesting that it is a general behavior for 2D phase-separating proteins containing IDRs (104). Increasing the NTA-lipid concentration, or increasing the NaCl concentration in the external milieu, promoted phase separation at the membrane surface and the appearance of tubes (104). The membrane tubes presented different morphologies (**Figure 5*b*,*c***), from unduloids with a wavy morphology in their contour to pearl necklace–like spherical buds connected by thin membrane necks, while others were cylindrical with thicknesses below the resolution limit (**Figure 5*c***). A continuum mechanics model was used to describe the tube morphology and its dependence on membrane bending (104). Tubes with undulating morphologies result from an area mismatch between the inner and outer leaflets of the bilayer (15), i.e., spontaneous curvature, and membrane bending occurs as a result of a compressive stress due to protein phase

Intrinsically disordered regions (IDRs): protein parts lacking a well-defined 3D (secondary) structure under physiological conditions

FUS (Fused in Sarcoma): a protein that is involved in various cellular processes, including RNA metabolism and stress response

separation maximizing the contact sites (overlap) of the protein and the membrane (104) (see **Figure 5*d***). The tube thickness was shown to be modulated by membrane bending rigidity via tuning of the lipid composition, salinity, or protein concentration (104). A parallel can be drawn to observations in ATPS vesicles, in which membrane wetting by the PEG-rich phase and polymer adsorption both trigger tube formation via the generation of spontaneous curvature (59), but the resulting curvatures are of opposite signs. Another analogy can be sought between the compressive forces exerted by protein 2D condensation (104), as in **Figure 5**, and the condensation effect of calcium ions adsorbing to charged membranes, resulting in tubulation and generation of spontaneous curvature of the same sign (1) (albeit without exhibiting phase separation).

BAR (Bin, amphiphysin, Rvs)-domain: a highly conserved protein domain forming a banana-shaped dimer structure acting as a scaffold for tubulation and differential curvature affinity

In contrast, lipid-anchored condensates of the membrane-bound BAR (Bin, amphiphysin, Rvs)-domain protein endophilin and its binding partner, lamellipodin, have been shown to mediate extensive adhesion of adjacent membranes and increase membrane tension (76). BAR-domain proteins are known to induce membrane curvature in several key biological processes (16, 89). However, how the formation of condensates can regulate the BAR-domain protein curvature generation remains an interesting open question (74).

The lipid-anchored condensates often appear to lack the 3D (bulk) nature of nonanchored membrane-bound condensates and may instead represent a molecular layer of the constituent biomacromolecules. Their 2D structure, reminiscent of a membrane domain, raises the open question of whether the composition of the membrane segment underneath the condensate is not drastically altered by locally concentrating the NTA lipids binding the condensate.

5. PHASE SEPARATION COUPLING AND EFFECT OF CONDENSATES ON MEMBRANE ORDER AND HYDRATION

Membranes not only serve as a barrier and a means of compartmentalization for the cell, but also exhibit complex and highly dynamic structures involved in many cellular functions, from signaling to trafficking and metabolism. Since the discovery of the lateral segregation of phospholipid membranes (86) and the proposal of the fluid mosaic model of the cell membrane (91), there has been continuous cross talk between studies performed on cells and biophysical studies on membrane models (9, 35, 38, 83). With the discovery of the liquid-ordered phase mediated by cholesterol by Hjort Ipsen and collaborators (42) and the raft hypothesis by Simons & Ikonen (88), the subcompartmentalization of membranes into domains with different properties has become a highly relevant topic in cell biology. During the 2000s, the study of liquid phase transitions in membranes was boosted by the first direct observation of membrane domains in GUVs (31). This was followed by studies of lipid mixture critical points (99) and the mechanical (28) and dynamical (8) properties of lipid domains. While there has not been any direct observation of micron-sized domains in the cell membrane (except in the yeast vacuolar membrane; 81), growing evidence suggests the existence of nanometer-scale transient domains involved in cell physiology (52). In this section, we discuss the coupling between phase separation in the membrane and protein phase separation processes and how the different phases can modulate each other.

5.1. Coupling Between Protein Condensation and Membrane Phase Separation

The raft hypothesis implies that protein clustering in the membrane could induce lipid condensation around it, suggesting that protein–protein interactions could modulate the lateral organization of the membrane (34, 82). With the discovery of membraneless organelles and phase separation in the cell cytoplasm, efforts to answer the question of whether the protein phase can influence the lipid phase state (and vice versa) quickly gained momentum. Protein phase separation at membrane surfaces has been proven to induce receptor clustering, promoting signaling (14, 43, 96). By using GUVs of a lipid mixture close to the miscibility point and lipid-anchored

proteins with strong interprotein interaction, Lee et al. (49) showed that protein phase separation at the GUV surface can promote lipid demixing. Later, Chung et al. (26) proved that, when the linker for activation of T cells (LAT) is reconstituted in GUVs together with Grb2 (growth factor receptor-bound 2) and the Ras activator Sos1 (son of sevenless 1), the phase separation of these proteins can mediate lipid domain formation. LAT undergoes reversible condensation upon tyrosine phosphorylation. When LAT condensates are formed at a melting temperature slightly above the miscibility temperature of the lipid mixture, they can induce lipid phase separation (26). Recently, Wang et al. (102) demonstrated, both in vitro and in cells, that there is thermodynamic coupling between the condensates formed by the phosphorylated intracellular domain of LAT (pLAT), Grb2, Sos1, and membrane-ordered domains. Wang et al. proved that the condensates can regulate the lipid phase state (**Figure 6*a***), and in turn, the lipid phase can stabilize protein condensation. This study clearly outlines the relevance and synergistic functionality of coupling between membrane and protein phase separation for signal transduction in immune cells (102).

LAURDAN [6-dodecanoyl-2-(dimethylamino) naphthalene]: an environmentally sensitive fluorescent probe responsive to the water dipolar relaxation and lipid packing around its moiety

Using coarse-grained molecular dynamics simulations, Shillcock et al. (85) proved that tridimensional droplets of intrinsically disordered proteins can promote the formation of lipid clusters on planar membranes, depending on the interaction affinity. Coupling of a bulk polymer-rich phase (as in an ATPS) to a specific membrane phase in GUVs has been demonstrated by the Keating group (4). Studying the dynamics of LLPS, Su et al. (95) showed that the PEG–dextran phase separation inside GUVs can drive membrane shape deformations and induce lipid phase separation (**Figure 6*b***).

Using free-standing planar bilayers formed on transmission electron microscopy (TEM) grids (48, 68, 72, 83), Lee et al. (51) showed that, when phase separation of lipid-anchored proteins occurs at both sides of the bilayer, transbilayer coupling of the protein phases can take place (**Figure 6*c***). This suggests that transbilayer coupling promoted by condensates could be a mechanism for interleaflet cross talk, which is of key relevance in signaling (51).

5.2. How Protein Condensates Affect Membrane Fluidity, Order, and Hydration

The condensates that wet membranes not only deform the membrane, but can also reduce the lipid mobility (51, 69) (see **Figure 6*d***). Interestingly, this reduction in lipid diffusion is not altered by the presence of interfacial ruffling (69) (see **Figure 3*b*,*f***).

Employing the phasor approach (66, 100) to analyze LAURDAN [6-dodecanoyl-2-(dimethylamino) naphthalene] hyperspectral and fluorescence lifetime imaging microscopy data, Mangiarotti et al. (70) proved that single-component lipid membranes in contact with condensates display increased lipid packing relative to and are more dehydrated than bare membranes (see **Figure 6*e–g***). Furthermore, when the wetting affinity increases, the membrane becomes more packed, and there is a reduction of the water dipolar relaxation (**Figure 6*f*,*g***). This was demonstrated both for protein- and for polymer-rich droplets with very different viscosities and interfacial tensions (69, 101), suggesting the existence of a general mechanism for modulating membrane order by condensate wetting (70). This effect could be related to the high concentration of macromolecules in the condensates; such macromolecular crowding was shown to affect lipid hydration, even producing mesomorphic transitions (67). Altogether, these results suggest that there is a strong relationship among protein organization, water activity, and membrane hydration that might be crucial for understanding phase separation in cell biology (10, 11, 70).

5.3. Some Words of Caution

In the case of 2D protein phase separation, when proteins are anchored to the membrane via NTA-lipids, the sorting of these lipids to the patches of phase-separated protein appears to form highly

packed lipid domains (51, 77), in some cases leading even to liquid-to-gel phase transition (77). For such systems, the clustering of NTA-lipids produces regions of composition distinct from the rest of the membrane, and it is unclear whether the observed effect is independent of the nature of the lipid anchor. In addition, the concentration of NTA-lipids on GUVs does not necessarily correspond to that of the starting lipid mixture and depends on the preparation method (80). This

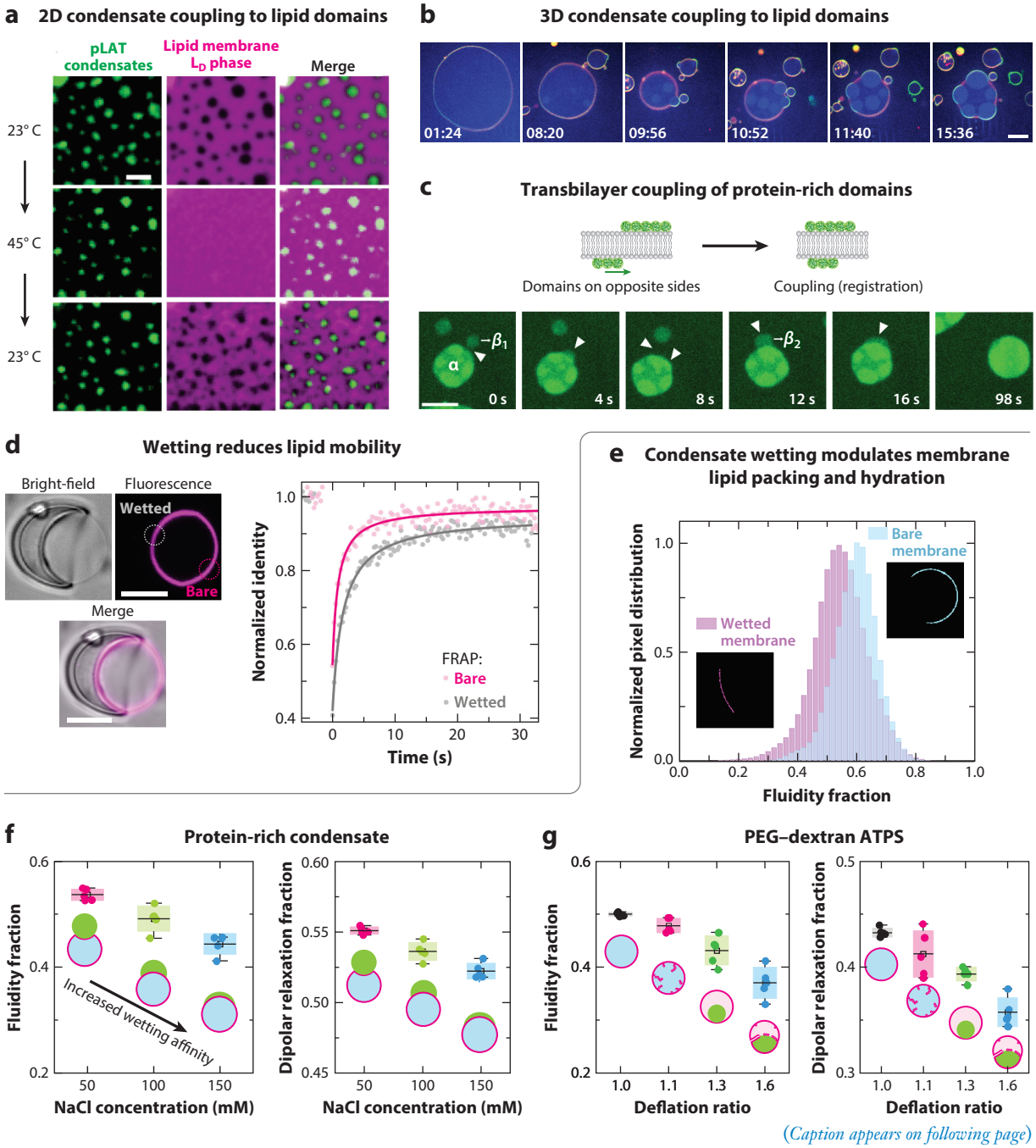

(*Caption appears on following page*)

Figure 6 (*Figure appears on preceding page*)

Coupling of the membrane phase state (domains), packing, and hydration with protein phase separation. (*a*) Preformed phosphorylated intracellular domain of the linker for activation of T cells (pLAT) condensates (*green*) template liquid-ordered (Lo) domain nucleation in supported multibilayers [the liquid-disordered (Ld) phase in the lipid membrane is shown in magenta; the fluorescent lipid marker is excluded from the Lo domains]. At 23°C, pLAT condensates colocalize with Lo domains. At 45°C, above the miscibility temperature of the lipids (approximately 37°C; for details, see 102), lipid mixing is observed, but protein condensates are not affected. Cooling back to 23°C induces formation of Lo domains colocalized with (i.e., templated by) the protein condensates. Scale bar is 5 μm. Panel adapted with permission from Reference 102. (*b*) Liquid–liquid phase separation (LLPS) inside giant unilamellar vesicles (GUVs) drives lipid domain coupling to specific polymer phases (95). Confocal fluorescence microscopy time-lapse images of GUVs encapsulating polyethylene glycol (PEG)–dextran aqueous two-phase systems (ATPSs) are shown upon osmotic deflation. The dextran-rich droplets (*blue*) protrude into buds that not only reshape the membrane, but also induce lipid demixing and membrane domain colocalization with the condensates. Scale bar is 10 μm. Panel provided by Wan-Chih Su and Atul N. Parikh. (*c*) Coupling of protein-rich domains (*green*) across the bilayer. The schematic and representative microscopic images over time show relocation and coupling of protein domains to spatially overlap across the membrane. The initially observed protein-rich region (α) is composed of domains with medium intensity (from protein-rich domains on one leaflet only) and domains with a brighter intensity (from apposing domains on both sides of the bilayer). Between 0 s and 8 s, the medium-intensity part of the α region and another smaller medium-bright region (β_1) overlap, producing a region with higher intensity and increased size, suggesting interleaflet coupling of the domains across the membrane. Similar coupling events were observed afterward (e.g., one more example between 12 s and 16 s), with full coupling occurring at 98 s, resulting in a region of juxtaposed domains (brighter intensity). The white arrowheads indicate coupling spots. Panel adapted from Reference 51 (CC BY 4.0). (*d*) Membrane wetting by condensates reduces the lipid mobility. For glycinin condensates wetting DOPC membranes, the recovery halftimes measured with fluorescence recovery after photobleaching (FRAP) show dynamics that are twice as slow in the membrane segment wetted by the condensate compared to the condensate-free (bare) membrane. Panel adapted from Reference 69 (CC BY 4.0). (*e–g*) Wetting by condensates tunes lipid packing and hydration. (*e*) On individual vesicles in contact with condensates, phasor analysis of hyperspectral images shows that the wetted membrane segment (*magenta*) displays increased lipid packing compared to the bare membrane (*cyan*). (*f,g*) Increasing wetting affinity of the droplet leads to increased lipid packing and reduced water dipolar relaxation in both (*f*) protein condensate and (*g*) PEG–dextran systems. (*f*) Raising the salinity increases the wetting affinity of glycinin condensates for DOPC GUVs, and this correlates with increasing lipid packing and reduced water dipolar relaxation. The schematics indicate the increase in membrane wetting by the protein condensates. (*g*) Increasing the polymer concentration inside a vesicle via deflation (the deflation ratio is the external versus the initial osmolarity) promotes membrane wetting by the condensate, leading to increased packing and reduced water dipolar relaxation. The schematics show the morphological transformations of vesicle encapsulation ATPSs and the increase in membrane wetting by the green polymer-rich phase. The fact that these two very different systems (in panels *f* and *g*) present the same behavior, despite the differences in interfacial tension and viscosities of the droplets, suggests a general mechanism for tuning membrane order by condensate wetting. Panels *e–g* adapted from Reference 70 (CC BY 4.0).

implies that extra caution should be taken when using these systems for quantitative evaluation of protein surface concentrations. Furthermore, the choice of a particular membrane model can influence the phase diagram of the lipid mixtures, depending on the degrees of freedom, restriction of out-of-plane motions, and presence of oil residues (19, 68, 71). This is likely to affect the phase behavior of anchored proteins and has yet to be addressed.

6. QUANTITATIVE DESCRIPTION OF MEMBRANE WETTING AND MOLDING

In this section, we briefly summarize concepts and approaches for quantifying wetting transitions and different morphologies of the vesicle droplet system shown in **Figures 1–3**. For a detailed compendium of the theoretical framework of membrane remodeling by droplets developed during the past two decades and scrutinized by experiments and simulations, the reader is referred to a recent review by Lipowsky (58). Extensive description of this topic is also provided in Lipowsky's (57) chapter in *The Giant Vesicle Book*.

6.1. Geometric Factor

To analyze the vesicle-droplet morphologies shown in **Figures 1–3**, it is necessary to consider the contact angles along the interfacial three-phase contact line among the interior solution

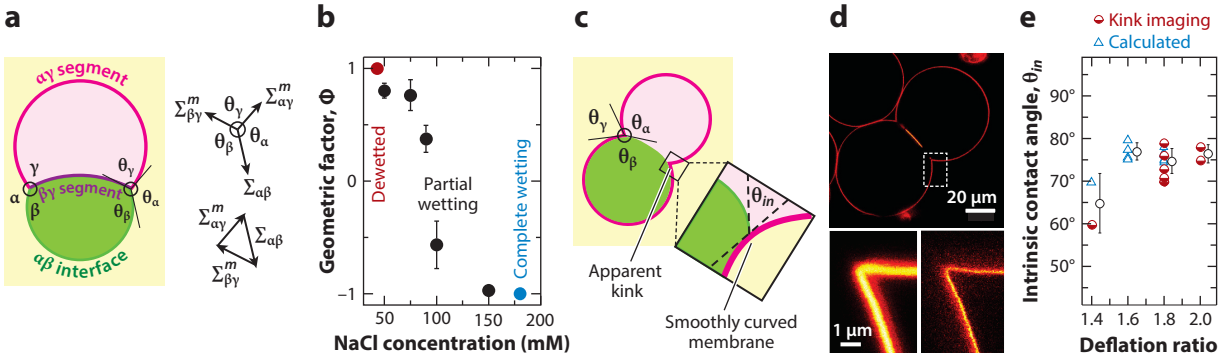

Figure 7

Quantitative description of membrane wetting and remodeling by condensates. (*a*) For partial wetting morphologies, the contact line between the condensate bare surface αβ and the membrane partitions the membrane into the αγ and βγ segments (*magenta* and *purple*, respectively), with the contact angles $\theta_\alpha + \theta_\beta + \theta_\gamma = 360°$. The force balance between the droplet interfacial tension $\Sigma_{\alpha\beta}$ and the mechanical tensions $\Sigma^m_{\alpha\gamma}$ and $\Sigma^m_{\beta\gamma}$ within the two membrane segments forms the sides of a triangle. (*b*) Experimental data for the geometric factor $\Phi = (\sin\theta_\alpha - \sin\theta_\beta)/\sin\theta_\gamma$ for glycinin condensates in contact with DOPC giant unilamellar vesicles (GUVs) as a function of NaCl concentration. The largest possible value, $\Phi = +1$ (*red circle*), corresponds to the transition from dewetting to partial wetting, and the smallest possible value, $\Phi = -1$ (*blue circle*), reflects the transition from partial wetting to complete wetting. The geometric factor characterizes the morphology of a vesicle-droplet system irrespective of the relative sizes of the vesicle and droplet. Panel adapted from Reference 69 (CC BY 4.0). (*c*) Schematic of a GUV enclosing an aqueous two-phase system (ATPS). The three-phase contact region is magnified, identifying the intrinsic contact angle θ_{in}. (*d*) Stimulated emission depletion (STED) image of a GUV enclosing an ATPS (*top*). Magnified confocal (*bottom left*) and 2D STED (*bottom right*) xy scans in the region are outlined by the dashed-lined rectangle in the top image. STED reveals that the apparent kink is a smoothly curved membrane. (*e*) Intrinsic contact angle measured at different deflation ratios (defined in **Figure 6**), as estimated from STED imaging of the kink region at the three-phase contact line (*red half-filled circles*) and as calculated from Equation 6 (*open blue triangles*). The mean values from both methods are shown with black open circles. Panels *d* and *e* adapted from Reference 108 (CC BY 4.0).

(γ, enclosed by the membrane *m*), the condensate (β), and the external solution (α), as shown in **Figure 7*a***. When measuring contact angles from confocal sections, it is important to remember that the confocal scan should cross the centers of the vesicle and condensate for the image to represent the correct contact angles. It is also not sufficient to measure only the contact angle θ_α between the membrane and the condensate; all three angles should be measured. Partial wetting morphologies involve three surface segments, αβ, βγ, and αγ, that meet along the contact line (45, 53, 56) (**Figure 7*a***). The contact angles are related to the different surface tensions that pull the segments along the contact line. The interfacial tension of the condensate–buffer interface, $\Sigma_{\alpha\beta}$, is balanced by the difference between the membrane tensions of the two membrane segments: $\Sigma^m_{\alpha\gamma} - \Sigma^m_{\beta\gamma}$, forming the sides of a triangle (also known as Neumann's triangle) (see **Figure 7*a***). The contact angles and the mechanical tensions of the two membrane segments depend on the lateral stress Σ within the membrane (56):

$$\Sigma^m_{\alpha\gamma} = \Sigma + W_{\alpha\gamma} \quad \text{and} \quad \Sigma^m_{\beta\gamma} = \Sigma + W_{\beta\gamma}, \qquad 1.$$

Neumann's triangle: relates the surface energies (interfacial tensions) and contact angles along a three-phase contact line

where $W_{\alpha\gamma}$ and $W_{\beta\gamma}$ represent the adhesion free energies per unit area of the respective interfaces (56). For simplicity, possible contributions from the spontaneous curvatures of the membrane segments are ignored (56). The adhesion parameter $W_{\beta\gamma}$ is positive if the membrane prefers the interior solution over the condensate, and it is negative otherwise. The affinity contrast between the condensate and the external buffer is then given by

$$W = \Sigma^m_{\beta\gamma} - \Sigma^m_{\alpha\gamma} = W_{\beta\gamma} - W_{\alpha\gamma} \quad \text{with} \quad -\Sigma_{\alpha\beta} \le W \le +\Sigma_{\alpha\beta}, \qquad 2.$$

where the inequalities follow from the tension triangle in **Figure 7*a***; each side of the triangle should be smaller than or equal to the sum of the two other sides. The limiting value $W = -\Sigma_{\beta\gamma}$ describes complete wetting by the condensate phase, whereas $W = +\Sigma_{\alpha\beta}$ corresponds to dewetting from the condensate phase (or complete wetting by the external buffer).

The relationships between the surface tensions and the contact angles can be derived from the tension triangle (56, 69):

$$\frac{\Sigma^m_{\alpha\gamma}}{\Sigma_{\alpha\beta}} = \frac{\Sigma + W_{\alpha\gamma}}{\Sigma_{\alpha\beta}} = \frac{\sin\theta_\beta}{\sin\theta_\gamma} \quad \text{and} \quad \frac{\Sigma^m_{\beta\gamma}}{\Sigma_{\alpha\beta}} = \frac{\Sigma + W_{\beta\gamma}}{\Sigma_{\alpha\beta}} = \frac{\sin\theta_\alpha}{\sin\theta_\gamma}. \qquad 3.$$

If we take the difference of these equations, the affinity contrast W in Equation 2 becomes equal to

$$W = \Phi\Sigma_{\alpha\beta} \quad \text{with} \quad \Phi \equiv \frac{\sin\theta_\alpha - \sin\theta_\beta}{\sin\theta_\gamma}. \qquad 4.$$

The rescaled affinity contrast is $\Phi = W/\Sigma_{\alpha\beta}$, in which W is a mechanical quantity related to the adhesion free energies of the membrane segments, a purely geometric quantity that can be obtained from the three apparent contact angles in the microscopy images (69) (**Figure 7*b***). The inequalities in Equation 2 imply $-1 \leq \Phi \leq 1$, where the limiting values of Φ correspond to the limiting cases for the affinity contrast W: The smallest possible value, $\Phi = -1$, corresponds to complete wetting of the membrane by the condensate phase, and the largest possible value, $\Phi = +1$, corresponds to dewetting. The dimensionless geometric factor Φ is negative if the membrane prefers the condensate over the exterior buffer, and it is positive otherwise. The value $\Phi = 0$ implies that $W = 0$, and there is no affinity contrast between the condensate and the external buffer. Lu et al. (65) also provided a model to characterize the morphologies of coacervates in contact with vesicles, but their description does not consider the affinity contrast and predicts only negative curvatures of the $\beta\gamma$ segment. The geometric factor is directly obtained by measuring the apparent angles from confocal images, but the correct projections should be considered (see 69). From the geometric factor Φ, measured as a function of one parameter that modifies the membrane–droplet interaction, e.g., the salinity or the membrane composition, the affinity contrast W can be obtained in units of the interfacial tension $\Sigma_{\alpha\beta}$ as a function of the given parameter (69). **Figure 7*b*** illustrates the effect of salinity on the geometric factor for glycinin condensates in contact with GUVs (such as those shown in **Figure 3**). Each point in the graph corresponds to a given vesicle-droplet morphology, and the sign of Φ indicates whether the membrane bulges toward the interior buffer ($\Phi < 0$) or toward the condensate ($\Phi > 0$) (69). Notably, the geometric factor is scale invariant and, consequently, does not depend on the size of a given vesicle and condensate pair.

6.2. Interfacial Ruffling

The emergence of ruffling and formation of finger-like protrusions (**Figure 3*f***) imply an increase in the bending energy (for negligible spontaneous curvature). To observe interfacial ruffling, this bending energy should be overcompensated for by the gain in adhesion energy for transferring membrane area from the $\alpha\gamma$ segment to the $\beta\gamma$ interface (see **Figure 7*a***). A simple criterion for the onset of ruffling was derived in Reference 69:

$$|\Phi|\,\Sigma_{\alpha\beta}\,\Delta A > 8\pi\kappa N_{pro}, \qquad 5.$$

where $|\Phi|$ is the absolute value of the geometric factor, ΔA represents the area transferred to the $\beta\gamma$ segment, κ is the bending rigidity, and N_{pro} is the number of protrusions observed.

6.3. Intrinsic Versus Microscopic Contact Angles and Apparent Membrane Kink

Typical confocal microscopy images of the adhesion morphologies suggest that the membrane exhibits a kink at the three-phase contact line (**Figure 7*c***). In the example in **Figure 7*c***, the condensate is inside the GUV (as in **Figures 1** and **2*b***), while in **Figure 7*a***, it is outside (as in **Figures 2*c*** and **3**); we conserve the notation of the different solutions with respect to the condensate (β) and its membrane-free interface (αβ). The observed sharp kink would imply infinite bending energy, and thus it cannot persist to the nanometer range (45, 108). At the nanometer scale, the membrane should be smoothly curved, exhibiting an intrinsic contact angle defining the membrane wetting and geometry (45) (see **Figure 7*c***). Using STED microscopy, Zhao et al. (108) resolved the smoothly curved membrane (**Figure 7*d***), showing that kinks are artifacts of low optical resolution. The intrinsic contact angle, θ_{in}, is a material parameter that can be related to the apparent microscopic angles through (45)

$$\cos\theta_{\text{in}} = \left(\sin\theta_{\alpha} - \sin\theta_{\beta}\right)/\sin\theta_{\gamma}. \qquad 6.$$

From Equation 4, it is obvious that the geometric factor and the intrinsic contact angle are related: $\Phi \equiv \cos\theta_{in}$. **Figure 7*e*** shows that there is a good agreement between the intrinsic contact angle estimated by STED images and the one calculated from confocal microscopy images using Equation 6.

7. OUTLOOK

Interactions between biomolecular condensates and membranes can produce their mutual remodeling. The droplets can spread on the membrane, increasing the contact surface and promoting wetting transitions. As a result of the interaction with the membrane, formation of endo- or exocytic buds, formation of nanotubular structures, membrane ruffling, and vesicle division can occur. While only a few remodeling processes have been described in cells to date, the potential of organelle reshaping by droplets suggests that there are many phenomena still to be discovered. Meanwhile, model (in vitro and in silico) systems provide valuable insight into the physicochemical principles governing membrane–condensate interactions that paves the way for the interpretation of the processes occurring in the complex cell environment. Bidimensional and tridimensional phase-separated proteins can organize membranes laterally, and the thermodynamic coupling of the protein and membrane phase separation can provide a synergetic mechanism for the regulation of signaling and information transmission. All of the results reviewed in this article were obtained from different model systems, suggesting that LLPS could be a general physicochemical principle driving mesoscale functional organization and coupling of membrane-bound and membraneless organelles in both living and artificial cells.

SUMMARY POINTS

1. Interaction between membranes and condensates can promote mutual remodeling processes, tuning of the membrane order, and coupling of the protein and membrane phase separation.
2. In vesicles in contact with aqueous two-phase systems, wetting transitions promote membrane budding, nanotube formation, and vesicle division. The individual polymer-rich phases can associate or colocalize to different lipid phases.

3. Synthetic coacervates provide an easy model of associative phase separation and can reshape the membrane through wetting transitions. Endocytosis and enzymatic reactions can take place in vesicle–coacervate systems, providing a convenient model for the development of synthetic cells and drug delivery systems.
4. Protein phase separation in bulk produces tridimensional droplets than can adhere to and wet membranes, reducing the diffusion of lipids. Wetting transitions lead to different morphologies than can be characterized by the geometric factor or the intrinsic contact angle, which are directly measured from the microscopic contact angles. Additionally, interaction of protein condensates with membranes can produce interfacial ruffling, bridging, and engulfment.
5. Lipid-anchored proteins can phase separate at membrane surfaces, triggering the formation of tubes as a consequence of compressive stress. This seems to be a general mechanism for proteins containing intrinsically disordered regions. In turn, proteins containing BAR-domains promote extensive membrane adhesion and increase membrane tension.
6. For anchored proteins, the lipid phase and the protein phase can be coupled: Existing domains can nucleate the protein phase, or previously formed condensates can recruit a nascent lipid phase. Moreover, protein condensates at different sides of the bilayer can be coupled.
7. For tridimensional droplets, the liquid–liquid phase separation inside vesicles can produce vesicle reshaping and phase separation of the lipid phase. For different membrane–droplet systems, a direct correlation between the wetting affinity and the degree of membrane lateral order is observed, suggesting that tuning membrane packing and hydration is a general mechanism for condensate wetting on membranes.

FUTURE ISSUES

1. Membrane interaction with condensates can alter the lipid mobility, but how the condensate dynamics are affected has not been explored.
2. The possibility of material exchange between the condensate and the membrane phase or between compartments like hollow condensates and the vesicle interior is still not understood.
3. Membrane penetration and crossing of condensates made of short polypeptides and oligonucleotides have been demonstrated, but it remains unclear whether these processes are relevant to membraneless organelles, or whether they apply mainly to developed drug-delivery systems.
4. We now have some understanding of the processes taking place at the mesoscale, but the influence of wetting on protein structure and the role of specific protein–lipid interactions have not been addressed.
5. Differences in membrane model systems have been shown to modify the phase diagram of the lipid mixtures. How the particular experimental model can influence the anchored protein phase behavior is an interesting question for future research.

6. The influence of electrostatics in coacervate systems interacting with membranes has been described; however, the influence of electrostatics is a more complex issue for protein condensates, since it can depend on the protein structure and the condensate charge density, and it remains to be addressed.

DISCLOSURE STATEMENT

The authors are not aware of any affiliations, memberships, funding, or financial holdings that might be perceived as affecting the objectivity of this review.

ACKNOWLEDGMENTS

A.M. acknowledges support from the Alexander von Humboldt Foundation. The authors thank R. Lipowsky for stimulating and insightful discussions on membrane mechanics and interactions with condensates.

LITERATURE CITED

1. Ali Doosti B, Pezeshkian W, Bruhn DS, Ipsen JH, Khandelia H, et al. 2017. Membrane tubulation in lipid vesicles triggered by the local application of calcium ions. *Langmuir* 33:11010–17
2. Alshareedah I, Moosa MM, Pham M, Potoyan DA, Banerjee PR. 2021. Programmable viscoelasticity in protein-RNA condensates with disordered sticker-spacer polypeptides. *Nat. Commun.* 12:6620
3. Alshareedah I, Moosa MM, Raju M, Potoyan DA, Banerjee PR. 2020. Phase transition of RNA–protein complexes into ordered hollow condensates. *PNAS* 117:15650–58
4. Andes-Koback M, Keating CD. 2011. Complete budding and asymmetric division of primitive model cells to produce daughter vesicles with different interior and membrane compositions. *J. Am. Chem. Soc.* 133:9545–55
5. Anila MM, Ghosh R, Różycki B. 2023. Membrane curvature sensing by model biomolecular condensates. *Soft Matter* 19:3723–32
6. Aumiller WM Jr., Pir Cakmak F, Davis BW, Keating CD. 2016. RNA-based coacervates as a model for membraneless organelles: formation, properties, and interfacial liposome assembly. *Langmuir* 32:10042–53
7. Babl L, Merino-Salomón A, Kanwa N, Schwille P. 2022. Membrane mediated phase separation of the bacterial nucleoid occlusion protein Noc. *Sci. Rep.* 12:17949
8. Bacia K, Scherfeld D, Kahya N, Schwille P. 2004. Fluorescence correlation spectroscopy relates rafts in model and native membranes. *Biophys. J.* 87:1034–43
9. Bagatolli LA, Ipsen JH, Simonsen AC, Mouritsen OG. 2010. An outlook on organization of lipids in membranes: searching for a realistic connection with the organization of biological membranes. *Prog. Lipid Res.* 49:378–89
10. Bagatolli LA, Mangiarotti A, Stock RP. 2021. Cellular metabolism and colloids: realistically linking physiology and biological physical chemistry. *Prog. Biophys. Mol. Biol.* 162:79–88
11. Bagatolli LA, Stock RP. 2021. Lipids, membranes, colloids and cells: a long view. *Biochim. Biophys. Acta Biomembr.* 1863:183684
12. Banani SF, Lee HO, Hyman AA, Rosen MK. 2017. Biomolecular condensates: organizers of cellular biochemistry. *Nat. Rev. Mol. Cell Biol.* 18:285–98
13. Banerjee PR, Milin AN, Moosa MM, Onuchic PL, Deniz AA. 2017. Reentrant phase transition drives dynamic substructure formation in ribonucleoprotein droplets. *Angew. Chem. Int. Ed.* 56:11354–59
14. Banjade S, Rosen MK. 2014. Phase transitions of multivalent proteins can promote clustering of membrane receptors. *eLife* 3:e04123
15. Bar-Ziv R, Moses E. 1994. Instability and "pearling" states produced in tubular membranes by competition of curvature and tension. *Phys. Rev. Lett.* 73:1392–95

16. **Bassereau P, Jin R, Baumgart T, Deserno M, Dimova R, et al. 2018. The 2018 biomembrane curvature and remodeling roadmap. *J. Phys. D* 51:343001**

16. Gives an overview of various means of generating and quantifying membrane curvature.

17. Bergeron-Sandoval L-P, Kumar S, Heris HK, Chang CLA, Cornell CE, et al. 2021. Endocytic proteins with prion-like domains form viscoelastic condensates that enable membrane remodeling. *PNAS* 118:e2113789118
18. Beutel O, Maraspini R, Pombo-García K, Martin-Lemaitre C, Honigmann A. 2019. Phase separation of zonula occludens proteins drives formation of tight junctions. *Cell* 179:923–36.e11
19. Blosser MC, Horst BG, Keller SL. 2016. cDICE method produces giant lipid vesicles under physiological conditions of charged lipids and ionic solutions. *Soft Matter* 12:7364–71
20. **Brangwynne CP, Eckmann CR, Courson DS, Rybarska A, Hoege C, et al. 2009. Germline P granules are liquid droplets that localize by controlled dissolution/condensation. *Science* 324:1729–32**

20. One of the first (seminal) papers promoting the idea of and providing evidence for biomolecular condensates as membraneless organelles.

21. Brangwynne CP, Tompa P, Pappu RV. 2015. Polymer physics of intracellular phase transitions. *Nat. Phys.* 11:899–904
22. Busch DJ, Houser JR, Hayden CC, Sherman MB, Lafer EM, Stachowiak JC. 2015. Intrinsically disordered proteins drive membrane curvature. *Nat. Commun.* 6:7875
23. Cans AS, Andes-Koback M, Keating CD. 2008. Positioning lipid membrane domains in giant vesicles by micro-organization of aqueous cytoplasm mimic. *J. Am. Chem. Soc.* 130:7400–6
24. Chen N, Zhao Z, Wang Y, Dimova R. 2020. Resolving the mechanisms of soy glycinin self-coacervation and hollow-condensate formation. *ACS Macro Lett.* 9:1844–52
25. Choi J-M, Holehouse AS, Pappu RV. 2020. Physical principles underlying the complex biology of intracellular phase transitions. *Annu. Rev. Biophys.* 49:107–33
26. Chung JK, Huang WYC, Carbone CB, Nocka LM, Parikh AN, et al. 2021. Coupled membrane lipid miscibility and phosphotyrosine-driven protein condensation phase transitions. *Biophys. J.* 120:1257–65
27. Crowe CD, Keating CD. 2018. Liquid–liquid phase separation in artificial cells. *Interface Focus* 8:20180032
28. Das S, Tian A, Baumgart T. 2008. Mechanical stability of micropipet-aspirated giant vesicles with fluid phase coexistence. *J. Phys. Chem. B* 112:11625–30
29. Day KJ, Kago G, Wang L, Richter JB, Hayden CC, et al. 2021. Liquid-like protein interactions catalyse assembly of endocytic vesicles. *Nat. Cell Biol.* 23:366–76
30. Deshpande S, Brandenburg F, Lau A, Last MGF, Spoelstra WK, et al. 2019. Spatiotemporal control of coacervate formation within liposomes. *Nat. Commun.* 10:1800
31. Dietrich C, Bagatolli LA, Volovyk ZN, Thompson NL, Levi M, et al. 2001. Lipid rafts reconstituted in model membranes. *Biophys. J.* 80:1417–28
32. Dimova R. 2014. Recent developments in the field of bending rigidity measurements on membranes. *Adv. Colloid Interface Sci.* 208:225–34
33. Dimova R, Lipowsky R. 2012. Lipid membranes in contact with aqueous phases of polymer solutions. *Soft Matter* 8:6409
34. Edidin M. 2001. Shrinking patches and slippery rafts: scales of domains in the plasma membrane. *Trends Cell Biol.* 11:492–96
35. Edidin M. 2003. The state of lipid rafts: from model membranes to cells. *Annu. Rev. Biophys. Biomol. Struct.* 32:257–83
36. Erkamp NA, Sneideris T, Ausserwöger H, Qian D, Qamar S, et al. 2023. Spatially non-uniform condensates emerge from dynamically arrested phase separation. *Nat. Commun.* 14:684
37. Ghosh R, Satarifard V, Lipowsky R. 2023. Different pathways for engulfment and endocytosis of liquid droplets by nanovesicles. *Nat. Commun.* 14:615
38. Goñi FM. 2014. The basic structure and dynamics of cell membranes: an update of the Singer-Nicolson model. *Biochim. Biophys. Acta Biomembr.* 1838:1467–76
39. Gouveia B, Kim Y, Shaevitz JW, Petry S, Stone HA, Brangwynne CP. 2022. Capillary forces generated by biomolecular condensates. *Nature* 609:255–64
40. Heinrich M, Tian A, Esposito C, Baumgart T. 2010. Dynamic sorting of lipids and proteins in membrane tubes with a moving phase boundary. *PNAS* 107:7208–13

41. Helfrich MR, Mangeney-Slavin LK, Long MS, Djoko Y, Keating CD. 2002. Aqueous phase separation in giant vesicles. *J. Am. Chem. Soc.* 124:13374–75
42. Hjort Ipsen J, Karlström G, Mourtisen OG, Wennerström H, Zuckermann MJ. 1987. Phase equilibria in the phosphatidylcholine-cholesterol system. *Biochim. Biophys. Acta Biomembr.* 905:162–72
43. Huang WYC, Yan Q, Lin W-C, Chung JK, Hansen SD, et al. 2016. Phosphotyrosine-mediated LAT assembly on membranes drives kinetic bifurcation in recruitment dynamics of the Ras activator SOS. *PNAS* 113:8218–23
44. Kilgore HR, Young RA. 2022. Learning the chemical grammar of biomolecular condensates. *Nat. Chem. Biol.* 18:1298–306
45. Kusumaatmaja H, Li Y, Dimova R, Lipowsky R. 2009. Intrinsic contact angle of aqueous phases at membranes and vesicles. *Phys. Rev. Lett.* 103:238103
46. Laghmach R, Alshareedah I, Pham M, Raju M, Banerjee PR, Potoyan DA. 2022. RNA chain length and stoichiometry govern surface tension and stability of protein-RNA condensates. *iScience* 25:104105
47. Last MGF, Deshpande S, Dekker C. 2020. pH-controlled coacervate–membrane interactions within liposomes. *ACS Nano* 14:4487–98
48. Lee H-R, Lee Y, Oh SS, Choi SQ. 2020. Ultra-stable freestanding lipid membrane array: direct visualization of dynamic membrane remodeling with cholesterol transport and enzymatic reactions. *Small* 16:2002541
49. Lee I-H, Imanaka MY, Modahl EH, Torres-Ocampo AP. 2019. Lipid raft phase modulation by membrane-anchored proteins with inherent phase separation properties. *ACS Omega* 4:6551–59
50. Lee JE, Cathey PI, Wu H, Parker R, Voeltz GK. 2020. Endoplasmic reticulum contact sites regulate the dynamics of membraneless organelles. *Science* 367:eaay7108
51. Lee Y, Park S, Yuan F, Hayden CC, Wang L, et al. 2023. Transmembrane coupling of liquid-like protein condensates. *Nat. Commun.* 14:8015
52. Levental I, Levental KR, Heberle FA. 2020. Lipid rafts: controversies resolved, mysteries remain. *Trends Cell Biol.* 30:341–53
53. Li Y, Kusumaatmaja H, Lipowsky R, Dimova R. 2012. Wetting-induced budding of vesicles in contact with several aqueous phases. *J. Phys. Chem. B* 116:1819–23
54. Li Y, Lipowsky R, Dimova R. 2008. Transition from complete to partial wetting within membrane compartments. *J. Am. Chem. Soc.* 130:12252–53
55. Li Y, Lipowsky R, Dimova R. 2011. Membrane nanotubes induced by aqueous phase separation and stabilized by spontaneous curvature. *PNAS* 108:4731–36
56. Lipowsky R. 2018. Response of membranes and vesicles to capillary forces arising from aqueous two-phase systems and water-in-water droplets. *J. Phys. Chem. B* 122:3572–86
57. Lipowsky R. 2019. Understanding giant vesicles—a theoretical perspective. In *The Giant Vesicle Book*, ed. R Dimova, C Marques, pp. 73–168. Boca Raton, FL: Taylor & Francis
58. Lipowsky R. 2023. Remodeling of biomembranes and vesicles by adhesion of condensate droplets. *Membranes* 13:223
59. Liu Y, Agudo-Canalejo J, Grafmüller A, Dimova R, Lipowsky R. 2016. Patterns of flexible nanotubes formed by liquid-ordered and liquid-disordered membranes. *ACS Nano* 10:463–74
60. Liu Y, Lipowsky R, Dimova R. 2012. Concentration dependence of the interfacial tension for aqueous two-phase polymer solutions of dextran and polyethylene glycol. *Langmuir* 28:3831–39
61. Long MS, Cans AS, Keating CD. 2008. Budding and asymmetric protein microcompartmentation in giant vesicles containing two aqueous phases. *J. Am. Chem. Soc.* 130:756–62
62. Long MS, Jones CD, Helfrich MR, Mangeney-Slavin LK, Keating CD. 2005. Dynamic microcompartmentation in synthetic cells. *PNAS* 102:5920–25
63. Love C, Steinkühler J, Gonzales DT, Yandrapalli N, Robinson T, et al. 2020. Reversible pH-responsive coacervate formation in lipid vesicles activates dormant enzymatic reactions. *Angew. Chem. Int. Ed.* 59:5950–57
64. Lu T, Hu X, van Haren MHI, Spruijt E, Huck WTS. 2023. Structure-property relationships governing membrane-penetrating behaviour of complex coacervates. *Small* 19:2303138
65. Lu T, Liese S, Schoenmakers L, Weber CA, Suzuki H, et al. 2022. Endocytosis of coacervates into liposomes. *J. Am. Chem. Soc.* 144:13451–55

52. Reviews concepts and controversies of the raft hypothesis and suggests approaches for understanding the physiological relevance of rafts.

54. The first work to report wetting transitions for condensates interacting with membranes.

57. Provides an extensive theoretical description of vesicle morphology and is part of a compendium of textbook-like material offering fundamentals for understanding membrane structure, properties, and behavior, including protocols and method descriptions.

58. Offers a detailed theoretical framework of membrane remodeling by condensates.

66. Malacrida L, Ranjit S, Jameson DM, Gratton E. 2021. The phasor plot: a universal circle to advance fluorescence lifetime analysis and interpretation. *Annu. Rev. Biophys.* 50:575–93
67. Mangiarotti A, Bagatolli LA. 2021. Impact of macromolecular crowding on the mesomorphic behavior of lipid self-assemblies. *Biochim. Biophys. Acta Biomembr.* 1863:183728
68. Mangiarotti A, Caruso B, Wilke N. 2014. Phase coexistence in films composed of DLPC and DPPC: a comparison between different model membrane systems. *Biochim. Biophys. Acta Biomembr.* 1838:1823–31
69. Mangiarotti A, Chen N, Zhao Z, Lipowsky R, Dimova R. 2023. Wetting and complex remodeling of membranes by biomolecular condensates. *Nat. Commun.* 14:2809
70. Mangiarotti A, Siri M, Tam NW, Zhao Z, Malacrida L, Dimova R. 2023. Biomolecular condensates modulate membrane lipid packing and hydration. *Nat. Commun.* 14:6081
71. Mangiarotti A, Wilke N. 2015. Energetics of the phase transition in free-standing versus supported lipid membranes. *J. Phys. Chem. B* 119:8718–24
72. Mangiarotti A, Wilke N. 2017. Electrostatic interactions at the microscale modulate dynamics and distribution of lipids in bilayers. *Soft Matter* 13:686–94
73. Mitrea DM, Mittasch M, Gomes BF, Klein IA, Murcko MA. 2022. Modulating biomolecular condensates: a novel approach to drug discovery. *Nat. Rev. Drug Discov.* 21:841–62
74. Mondal S, Baumgart T. 2023. Membrane reshaping by protein condensates. *Biochim. Biophys. Acta Biomembr.* 1865:184121
75. Mondal S, Cui Q. 2022. Coacervation of poly-electrolytes in the presence of lipid bilayers: mutual alteration of structure and morphology. *Chem. Sci.* 13:7933–46
76. Mondal S, Narayan K, Botterbusch S, Powers I, Zheng J, et al. 2022. Multivalent interactions between molecular components involved in fast endophilin mediated endocytosis drive protein phase separation. *Nat. Commun.* 13:5017
77. Nixon-Abell J, Ruggeri FS, Qamar S, Herling TW, Czekalska MA, et al. 2023. ANXA11 biomolecular condensates facilitate protein-lipid phase coupling on lysosomal membranes. bioRxiv 2023.03.22.533832. **https://doi.org/10.1101/2023.03.22.533832**
78. Pir Cakmak F, Grigas AT, Keating CD. 2019. Lipid vesicle-coated complex coacervates. *Langmuir* 35:7830–40
79. Pir Cakmak F, Marianelli AM, Keating CD. 2021. Phospholipid membrane formation templated by coacervate droplets. *Langmuir* 37:10366–75
80. Pramanik S, Steinkühler J, Dimova R, Spatz J, Lipowsky R. 2022. Binding of His-tagged fluorophores to lipid bilayers of giant vesicles. *Soft Matter* 18:6372–83
81. Rayermann SP, Rayermann GE, Cornell CE, Merz AJ, Keller SL. 2017. Hallmarks of reversible separation of living, unperturbed cell membranes into two liquid phases. *Biophys. J.* 113:2425–32
82. Reigada R, Lindenberg K. 2011. Raft formation in cell membranes: speculations about mechanisms and models. *Adv. Planar Lipid Bilayers Liposomes* 14:97–127
83. Rosetti CM, Mangiarotti A, Wilke N. 2017. Sizes of lipid domains: What do we know from artificial lipid membranes? What are the possible shared features with membrane rafts in cells? *Biochim. Biophys. Acta Biomembr.* 1859:789–802
84. Rouches M, Veatch SL, Machta BB. 2021. Surface densities prewet a near-critical membrane. *PNAS* 118:e2103401118
85. Shillcock JC, Thomas DB, Beaumont JR, Bragg GM, Vousden ML, Brown AD. 2022. Coupling bulk phase separation of disordered proteins to membrane domain formation in molecular simulations on a bespoke compute fabric. *Membranes* 12:17
86. Shimshick EJ, McConnell HM. 1973. Lateral phase separation in phospholipid membranes. *Biochemistry* 12:2351–60
87. Shin Y, Brangwynne CP. 2017. Liquid phase condensation in cell physiology and disease. *Science* 357:eaaf4382
88. Simons K, Ikonen E. 1997. Functional rafts in cell membranes. *Nature* 387:569–72
89. Simunovic M, Voth GA, Callan-Jones A, Bassereau P. 2015. When physics takes over: BAR proteins and membrane curvature. *Trends Cell Biol.* 25:780–92
90. Sing CE. 2017. Development of the modern theory of polymeric complex coacervation. *Adv. Colloid Interface Sci.* 239:2–16

69. Describes a broad spectrum of the remodeling processes driven by wetting of 3D protein condensates.

91. Singer SJ, Nicolson GL. 1972. The fluid mosaic model of structure of cell membranes. *Science* 175:720–31
92. Snead WT, Gladfelter AS. 2019. The control centers of biomolecular phase separation: how membrane surfaces, PTMs, and active processes regulate condensation. *Mol. Cell* 76:295–305
93. Snead WT, Jalihal AP, Gerbich TM, Seim I, Hu Z, Gladfelter AS. 2022. Membrane surfaces regulate assembly of ribonucleoprotein condensates. *Nat. Cell Biol.* 24:461–70
94. Steinkühler J, Sezgin E, Urbančič I, Eggeling C, Dimova R. 2019. Mechanical properties of plasma membrane vesicles correlate with lipid order, viscosity and cell density. *Commun. Biol.* 2:337
95. Su W-C, Ho JCS, Gettel DL, Rowland AT, Keating CD, Parikh AN. 2024. Kinetic control of shape deformations and membrane phase separation inside giant vesicles. *Nat. Chem.* 16:54–62
96. Su X, Ditlev JA, Hui E, Xing W, Banjade S, et al. 2016. Phase separation of signaling molecules promotes T cell receptor signal transduction. *Science* 352:595–99
97. Tang T-YD, Che Hak CR, Thompson AJ, Kuimova MK, Williams DS, et al. 2014. Fatty acid membrane assembly on coacervate microdroplets as a step towards a hybrid protocell model. *Nat. Chem.* 6:527–33
98. Updike DL, Hachey SJ, Kreher J, Strome S. 2011. P granules extend the nuclear pore complex environment in the *C. elegans* germ line. *J. Cell Biol.* 192:939–48
99. Veatch SL, Keller SL. 2005. Seeing spots: complex phase behavior in simple membranes. *Biochim. Biophys. Acta Mol. Cell Res.* 1746:172–85
100. Vorontsova I, Vallmitjana A, Torrado B, Schilling TF, Hall JE, et al. 2022. In vivo macromolecular crowding is differentially modulated by aquaporin 0 in zebrafish lens: insights from a nanoenvironment sensor and spectral imaging. *Sci. Adv.* 8:eabj4833
101. Wang H, Kelley FM, Milovanovic D, Schuster BS, Shi Z. 2021. Surface tension and viscosity of protein condensates quantified by micropipette aspiration. *Biophys. Rep.* 1:100011
102. Wang H-Y, Chan SH, Dey S, Castello-Serrano I, Rosen MK, et al. 2023. Coupling of protein condensates to ordered lipid domains determines functional membrane organization. *Sci. Adv.* 9:eadf6205
103. Wang J, Choi J-M, Holehouse AS, Lee HO, Zhang X, et al. 2018. A molecular grammar governing the driving forces for phase separation of prion-like RNA binding proteins. *Cell* 174:688–99.e16
104. Yuan F, Alimohamadi H, Bakka B, Trementozzi AN, Day KJ, et al. 2021. Membrane bending by protein phase separation. *PNAS* 118:e2017435118
105. Zhang C, Rabouille C. 2019. Membrane-bound meet membraneless in health and disease. *Cells* 8:1000
106. Zhang Y, Chen Y, Yang X, He X, Li M, et al. 2021. Giant coacervate vesicles as an integrated approach to cytomimetic modeling. *J. Am. Chem. Soc.* 143:2866–74
107. Zhao X, Bartolucci G, Honigmann A, Jülicher F, Weber CA. 2021. Thermodynamics of wetting, prewetting and surface phase transitions with surface binding. *New J. Phys.* 23:123003
108. Zhao Z, Roy D, Steinkühler J, Robinson T, Lipowsky R, Dimova R. 2021. Super-resolution imaging of highly curved membrane structures in giant vesicles encapsulating molecular condensates. *Adv. Mater.* 34:2106633

101. Provides an overview of data in the literature, including values of the interfacial tension and viscosity of various macromolecular condensates.

102. Shows the thermodynamic coupling of protein and lipid phase separation in vitro and in cells.

104. Provides the first systematic study of 2D protein phase separation and membrane remodeling.